Experimental Characterization of the Dimensional Stability of Deployable Composite Booms During Stowage

Joshua E. Salazar[1] and Juan M. Fernandez[2]
NASA Langley Research Center, Hampton, VA, 23681

Thin-ply carbon fiber reinforced polymer materials offer the opportunity to create long thin-shell booms with high strength to weight ratios. These booms can be rolled up and stowed in small volumes to be later deployed. These features make them ideal for use in gossamer solar sails as well as other deployable space structures. It has been observed that stowing the booms in rolled-up configurations can cause time-dependent deformations. A comprehensive understanding of the detrimental effects of stowing the coiled booms is necessary to implement these structures in spaceflight missions. During stowage inside the spacecraft, the boom is subjected to a constant deformation/strain that causes it to relax over time, measurable by a decrease in stress. Using large deformation bending tests, the complete fold-stow-unfold-recover cycle of thin-laminate candidates for the rollable booms is characterized. Further bending and stowage testing is done at the boom level. The results from this test campaign will be used to evaluate the dimensional stability of deployable booms made from thin-ply composites that exhibit visco-elasto-plastic behavior and calibrate and validate numerical finite element models that include visco-elasto-plastic material models.

Nomenclature

E_r	=	Relaxation Modulus
ρ	=	Time constant
E_1	=	Young's Modulus in longitudinal direction
E_2	=	Young's Modulus in transverse direction
v_{12}	=	Poison Ratio
G_{12}	=	Shear Modulus
D_{11}	=	Bending Stiffness in longitudinal direction
D^*_{11}	=	Effective Bending Stiffness in longitudinal direction
a_T	=	Shift Factor
t_r	=	Thickness
t	=	Time
T	=	Temperature (°C)
M	=	Applied Moment
P	=	Applied Load
s	=	Coupon Gauge Length
l	=	CBT fixture length
r	=	Moment arm
ϕ	=	CBT coupon rotation angle
θ	=	CBT initial offset angle
R_1	=	Radius of shell segment 1
R_2	=	Radius of shell segment 2

[1] PhD Student, University of Texas at Dallas, Pathways Student Trainee, Structural Dynamics Branch, NASA LaRC, 2 West Bush Road, MS 497.
[2] Research Aerospace Engineer, Structural Dynamics Branch, NASA LaRC, 4 West Taylor St, MS 230. AIAA Member.

I. Introduction

Spread-tow carbon fiber has allowed for the design of thin-ply carbon fiber reinforced polymer (CFRP) composites. With thinner plies a CFRP composite can be manufactured with multiple layers and fiber orientations, taking advantage of the benefits of combining different weave patterns, while still having an overall thin gauge needed for compact stowage. This gives access to much thinner and more flexible composite structures that have a higher strength-to-weight ratio than their thicker counterparts [1]. These thinner composite structures have proven useful for deployable structures, which have many applications in space structures. Thin-ply deployable composites are currently being used for boom structures in solar sails and drag sails [1, 2]. They also have many more applications including deployable antennas, deployable panels/surfaces, as well as thin parabolic reflectors [3]. These thin structures have advantages over other materials like metals because of their low thermal expansion and thermal conductive properties. In-space thermal fluctuations can be detrimental to thin structures, causing undesirable deformations in metals that would be reduced by using CFRPs [4]. When stowed in a coiled configuration and constant deformation, the composite booms undergo time-dependent deformations due to the relaxation of the polymer matrix. An example of the deployable composite boom (DCB) partially rolled can be seen in Fig 1 (b). The Collapsible Tubular Mast (CTM) boom is the focus of this work. The CTM closed cross-section is formed by bonding together two omega-shaped shells . The two radii shown in Fig. 1 (a) of the omega shape are critical dimensions when designing the booms and when observing deformations in the booms. The two flat regions, called the web, also shown in Fig. 1 (a), is where the omega shells are bonded together with an epoxy adhesive. Fig. 1 (c) and 1 (d) show the stowage of a 16.5-meter boom around a spool with a resulting outer diameter of 230 millimeters. These booms have been observed to retain deformation after one month of stowage. This partially recovered deformation can be seen in Fig 2. for a previous boom laminate architecture no longer in use and prone to creep. The flattening of the boom shown after prolonged stowage could lead to a decrease in the buckling load of the boom by up to 50 percent. It reflects how important an adequate laminate design is to the long-term viability of thin shell rollable booms.

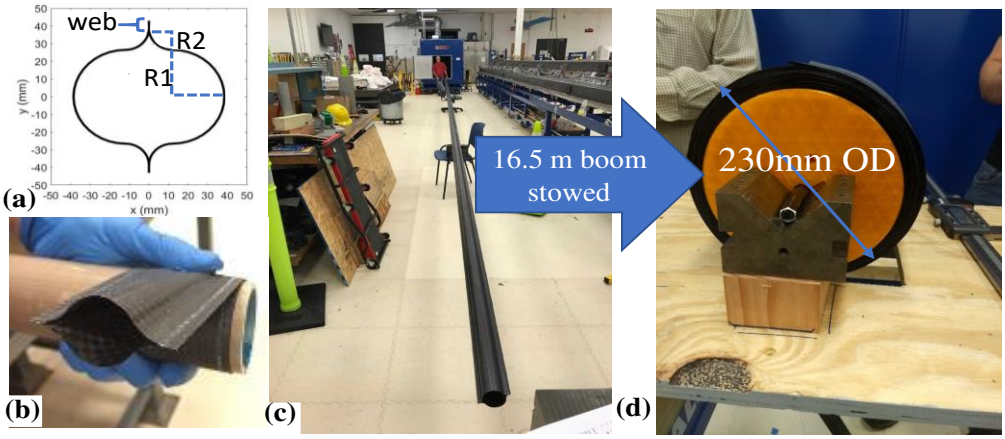

Fig. 1 CTM-type deployable composite booms: (a) cross section of a CTM style DCB showing the critical design dimensions. (b) partially rolled CTM boom. (c) 16.5-meter-long boom (d) 16.5 meter boom rolled on to a hub with an

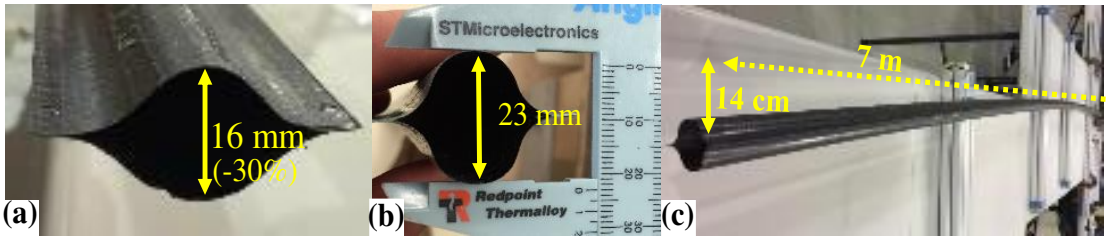

Fig. 2 CTM boom deformations post-stowage: (a), (b) distorted cross section of CTM booms after a month of stowage. (c) Longitudinal distortion of a CTM boom after a month of stowage

The loss of strain energy during storage may also impair the self-deployment capability of the boom and prevent full extension [5]. These slender deployable booms can pack into very small volumes, as shown in Fig. 1 (c) and Fig. 1 (d), but their effective application depends on a strong understanding of their dimensional stability while stowed [6]. Considerations of the viscoelastic effects in thin-shell composites have been conducted previously on structures in the form of tape springs [7,8]. These multiscale studies present viscoelastic micromechanics models of plain weave (PW) composites in order to determine the macroscopic relaxation effects in tape springs. A similar multiscale approach can

be applied to the more complicated geometries of deployable composite booms like the CTM [9]. In order to develop these models, the material and structural properties of the composite booms need to be determined using viscoelastic and viscoplastic characterization testing methods. In this work, tensile relaxation testing was performed on the polymer matrix used in the composite as well as the polymer adhesive that bonds together the two omega-shaped thin-shells of the booms. Bending relaxation testing was conducted on the composite laminates of interest at the coupon/material level. Finally, testing for relaxation response was performed at the structural level by testing sections of composite booms as well as full-scale boom structures.

II. Polymer Tensile Relaxation Testing

A. Polymer Adhesive

During DCB manufacture, the thin gauge sections are bonded together to achieve a closed cross-section geometry that has increased stiffness properties. The bond adhesives are polymers that will relax over time when subjected to a constant strain. High shear stresses have been observed at the web. Characterizing how this shear stress and the time depended properties of the adhesive affect each other can help evaluate the risks of using this technology. Table 1 shows the properties of the polymers of interest, Hysol EA 9696 film epoxy and PMT-F7 toughened epoxy resin. Thin films of the EA9696 adhesive were cured in an autoclave and then laser cut into standard dog-bone shapes for tensile relaxation tests.

Table 1. Polymer material properties used in the deployable composite booms of this study

Material Description	Width (mm)	Thickness (mm)	E (GPa)	Vendor
Hysol EA 9696	12.7	0.14	1.8	Henkel
PMT-F7	12.7	4	2.5	PatzM&T

After cut, the dog bones were speckled with black spray paint or a black marker. The speckle pattern is necessary for digital image correlation (DIC). DIC will allow the measurement of large three-dimensional deformation fields. The sample was clamped by tensile grips to perform the tensile relaxation test at temperatures increasing from 40 ºC to 80 ºC in 10 ºC increments. The chamber was given 92 minutes to reach thermal equilibrium at each temperature. The dog bones were pulled to a displacement of 10.16 mm at at rate of 10.16 mm per minute. The displacement was held for 6 hours followed by a zero-load creep recovery step. Figure 3 (a) shows the test setup with the DIC cameras directed at the speckled test specimen through a window in the thermal chamber. Fig. 3 (b) shows a view from the camera.

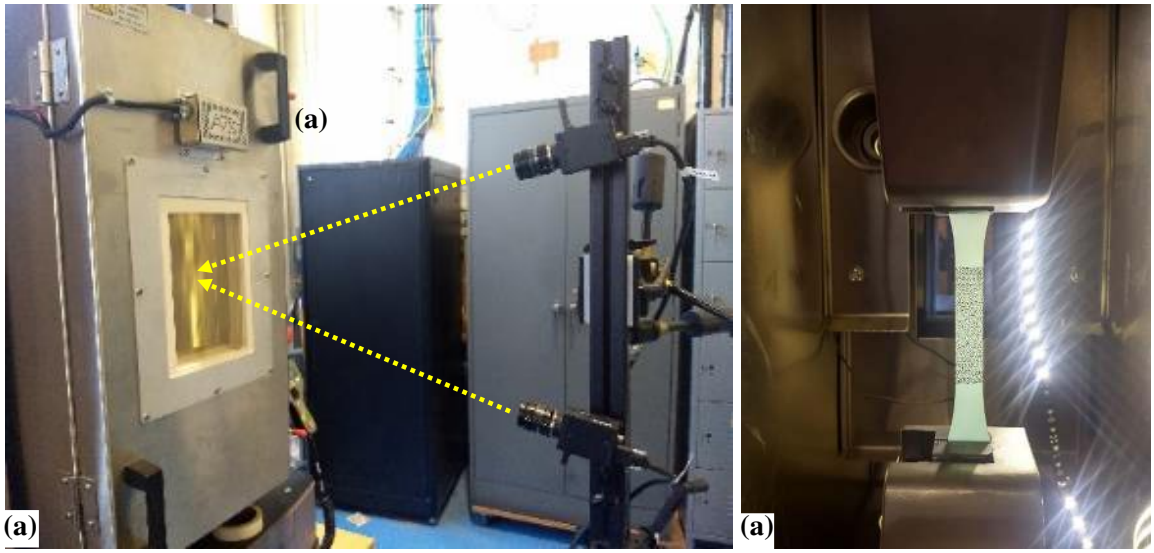

Fig. 3 Polymer relaxation testing setup: (a) Stereo camera setup for DIC deformation tracking. (b) stereo camera view of EA 9696 test dog bone

Figure 4 shows the relaxation modulus for the EA 9696 adhesive test. The relaxation modulus is the response of a material to stress and strain over time. As expected, the modulus reduced with increasing temperature and decreased with time. Assuming the material is thermorheologically simple, the time temperature superposition principle (TTSP) could be used to shift the relaxation modulus curves relative to the one at 40 ºC and build a master curve that represents a much longer relaxation time at 40 ºC. The shift factors used for the time shift are shown in Fig. 4 (c). These shift factors were determined from the amount that time was scaled, for their respective temperatures, in the logarithmic-time domain.

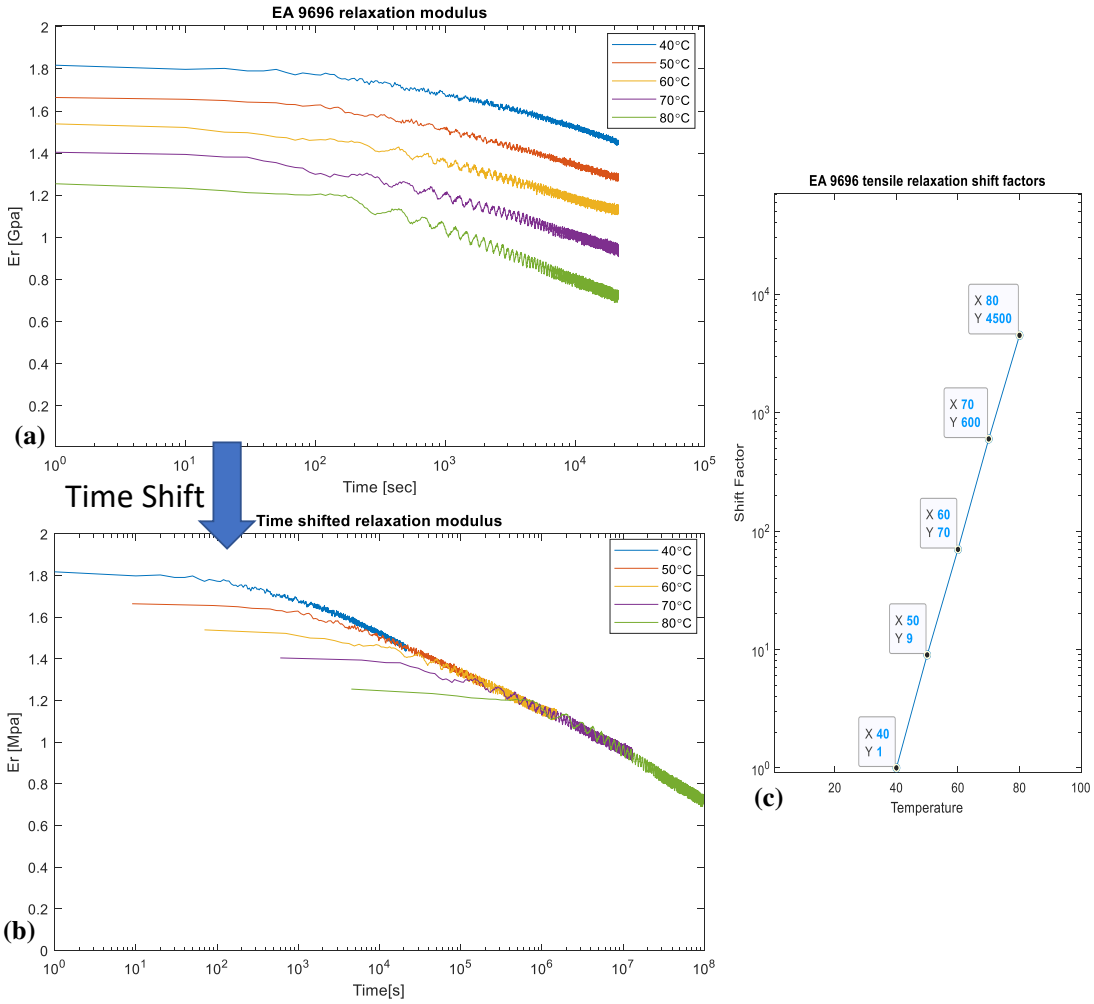

Fig. 4 EA 9696 adhesive relaxation modulus time shift: (a) Graph of EA9696 relaxation moduli for temperatures 40-80 ºC. (b) Graph of the relaxation moduli shifted in time relative to 40ºC. (c) Graph showing the linear relationship between the logarithmic time shift factors and temperature that were used to shift the graph in (b)

After a master curve was created a Prony series was fitted to the experimental data using a least squares approach. Equation 1 shows the Prony series that is used. The coefficients E_r and ρ were determined for each respective k^{th} term. The first term of the series, $E_{r,\infty}$, is the steady state relaxation modulus and is equivalent to $E_{r,k=0}$. Fig. 5 (a) shows the results of the least squares fit to Equation 1. Fig. 5b shows the log-time plot and the coefficients obtained from the least squares fit. A black dotted vertical line is marked on the graph at two years. Two years was assumed to be the upper limit stowage time for these deployable composites for current applications of interest to NASA. The experimental data and the fitted Prony series extend past this time frame.

$$E_r = E_{r,\infty} + \sum_{k=1}^{n} E_{r,k} * e^{-\frac{t}{\rho_k}} \quad (1)$$

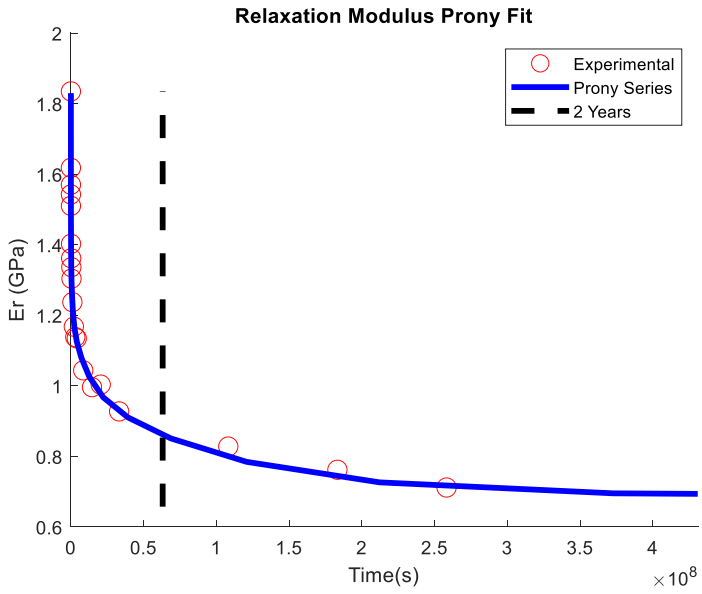

(a)

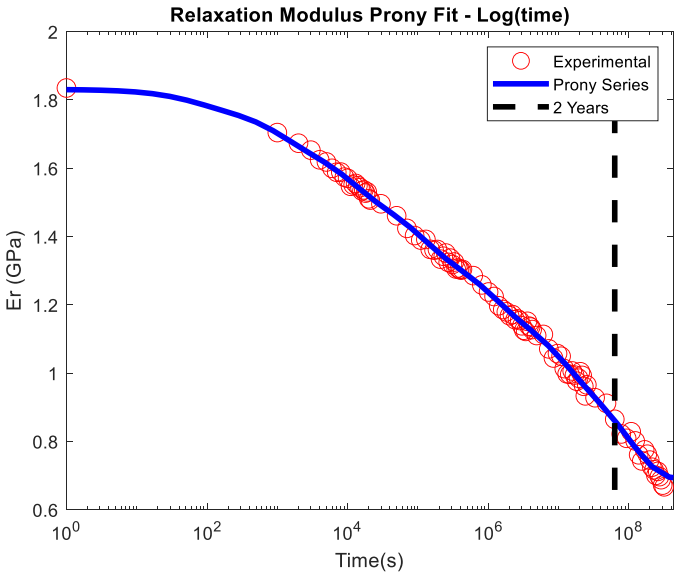

k	E_r [Mpa]	ρ
0	0.6875	NaN
1	1.81E-06	0.8227
2	0.0472	65.9555
3	0.1028	999.156
4	0.1489	10003
5	0.1687	99999
6	0.1663	1000000
7	0.1848	10000000
8	0.3246	1E+08

(b)

Fig. 5 EA 9696 adhesive relaxation modulus master curve and Prony fit: (a) Prony series fit to the experimental data shown in Fig. 4. (b) Prony series fit on a logarithmic time scale with the coefficients of the Prony series

B. Polymer Matrix

It is important to characterize the time-dependent relaxation properties of the polymer matrix because the carbon fibers are highly elastic. The polymer matrix is the main cause for any time-dependent relaxation effects in the

composite. As a result, laminate architecture and fiber orientation also have a significant effect as how the resin is loaded [10]. The tensile relaxation testing for the polymer matrix was performed in a similar way as the adhesive testing. A strain/displacement was applied to the polymer in a tensile test setup and held constant while the polymer relaxes over time. This was carried out at increasing temperatures starting at 40 ºC and increasing to 70 ºC in 10 ºC increments with a relaxation time of 3 hours.

Assuming the polymer is thermorheologically simple, the TTSP was used to construct a relaxation modulus master curve at the reference temperature of 40ºC shown in Fig. 6. Further tests are needed at higher temperatures to increase the time represented in the 40ºC master curve to beyond a few days shown in the graph. The data was fitted with a Prony series using Eq. 1. The tensile relaxation response of the polymer matrix was used to develop micromechanics models for the composites that will be applied to the booms to predict the dimensional stability of the booms during long-term stowage.

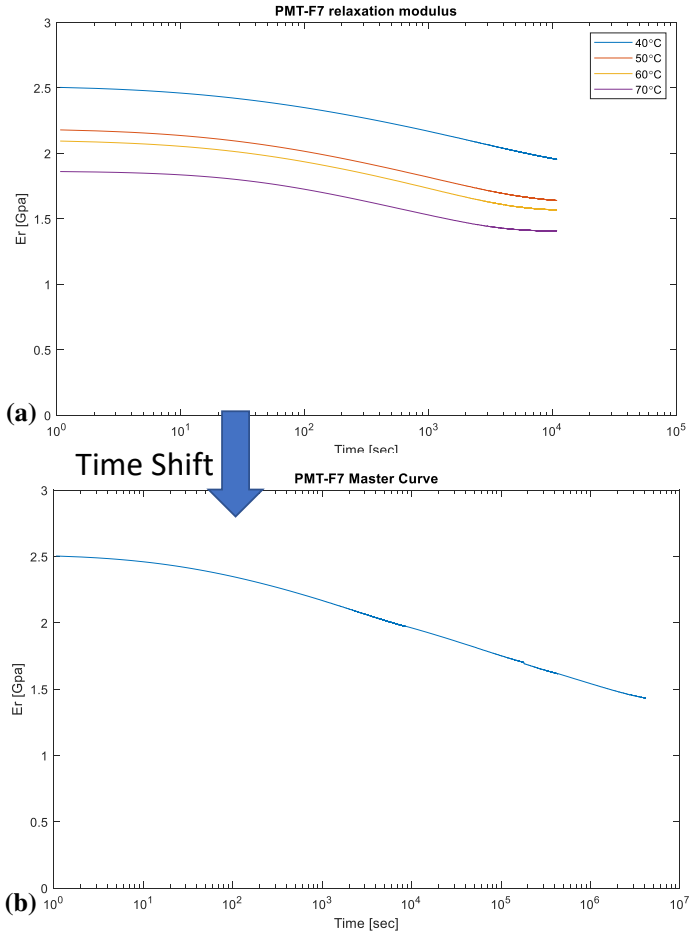

Fig. 6 PMT-F7 relaxation modulus time shift: (a) Relaxation moduli of PMT-F7 from 40ºC to 70ºC. (b) Master curve made from time shifting the relaxation moduli relative to 40ºC

III. Composite Bending Relaxation Testing

The combination of carbon fiber with a polymer matrix creates an anisotropic composite material. This causes the relaxation properties of the polymer matrix to be reduced by the highly elastic carbon fibers. Understanding the relaxation response during bending of the thin-ply composites at a coupon/material level will help to validate and calibrate micromechanical models being developed. The complete operational cycle of the boom, which includes stowage of the boom, can then be modeled accurately [9-11]. Thin-ply and thin-shell composites can sustain large bending deformations and strains. To study the composites at these large bending strain regimes, a test suitable method was developed called the Column Bending Test (CBT) [12]. This test method overcomes the limitations of traditional testing methods such as three-point and four-point bending that are not designed to handle the thin composite high deformations [12]. Other test methods for high deformation bending are the simple vertical test, bending platen test,

and the large-deformation four-point bending (LD-FBD) test. The simple vertical test with tape hinges is prone to gravity-induced lateral loads and moments that tend to produce coupon/tape shear distortion at large rotation angles or induced curvatures. The platen test generates a small localized region of high curvature in coupon apex, well away from coupon ends, that result in uncharacteristically high failure curvatures. The moment and stress over the coupon are highly non-uniform requiring complex structural analyses to interpret test results. The platen test is used for determining an upper limit on maximum coupon curvature or for computing strains and stresses at failure, butis not used to assess bending stiffness as it does not represent a pure bending state accurately. Large Deformation Four-Point Bending (LD-FPB) subjects the coupon to a pure bending stress state and is used to measure bending stiffness, including fiber nonlinear effects. However, the abrupt transition from flat to curved creates stress concentrations at the grip, which cause premature failure at the grips and not in the test section. Therefore, LD-FPB is not normally used for bending strength and strain to failure evaluation [12].

The CBT was developed at Opterus R&D and evaluated and improved at the NASA Langley Research Center (LaRC) [12]. Other researchers have successfully used CBT to characterize the bending stiffness/strength of thin laminates [13]. The CBT has some of the benefits of the three tests mentioned earlier without having some of the drawbacks of large deformation bending tests. This test method applies a moment across the test specimen that increases from the grips to the center of the test specimen, with the center having the highest moment and curvature. The moment gradient is known and is small across the specimen, but it ensures the failure of the coupon at the center of the specimens and not at the grips. This gives the ability to test thin composites over a full range of curvatures up to failure. The fixture is counterbalanced, meaning it is symmetric about the point it is pinned so that gravity has no effect on the test fixtures.

This test method has simple kinematics used to calculate the moment and bending stiffness of a coupon from the load and displacement data from a load frame. Equations 2-6 show the kinematic relationship and can be solved numerically for the moment. This test method was originally intended to study the failure of thin composites at high bending deformations [12]. The CBT fixtures were additively manufactured out of common high-temperature 3D-printed plastics such as Polylactic (PLA) and Acrylonitrile Butadiene Styrene (ABS).. Figure 7 shows the weight-balanced, high-temperature CBT fixture folding a thin flexure and the idealization (free body diagram) showing all the test parameters involved. In this paper, the CBT method was used to study the bending relaxation response of various laminates under consideration for deployable composite booms. The CBT test fixture was additively manufactured out of titanium to avoid relaxation effects observed on the previous plastic fixtures when used for coupon bending relaxation characterization.

$$\frac{\delta}{s} = 1 - \frac{2}{\phi}\sin\frac{\phi}{2} + 2\frac{l}{s}\left(\cos\theta - \cos\left(\theta + \frac{\phi}{2}\right)\right) \tag{2}$$

$$\kappa = \frac{\phi}{s} \tag{3}$$

$$\frac{r}{s} = \frac{1}{\phi}\left(1 - \cos\frac{\phi}{2}\right) + \frac{l}{s}\sin\left(\theta + \frac{\phi}{2}\right) \tag{4}$$

$$M_{max} = Pr \tag{5}$$

$$M_{min} = Pl\,sin\left(\theta + \frac{\phi}{2}\right) \tag{6}$$

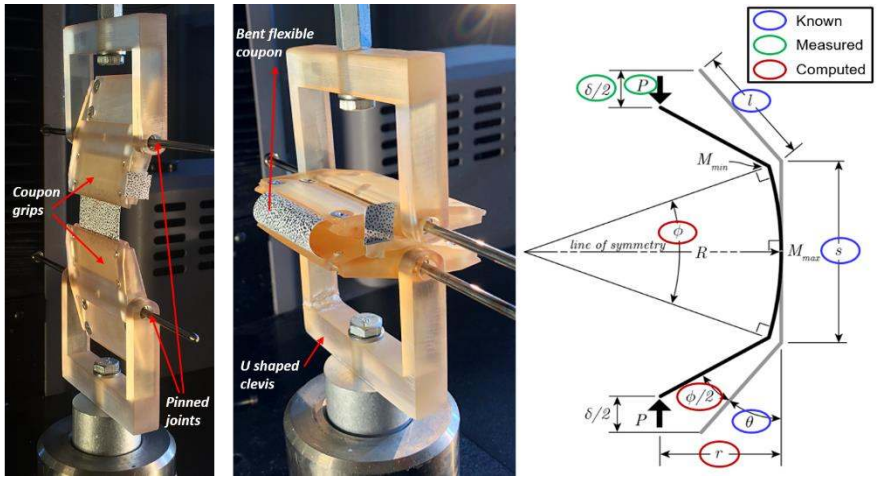

Fig. 7 Column Bending Test (CBT): (left) images of the column bending test at its initial position with a test coupon clamped. (middle) Image of the CBT at its max rotation, folding the coupon about 180 digress. (right) Diagram of the important dimensions of the CBT used in the kinematic analysis (equations 2-6).

Table 2 and Table 3 show the thin-ply composite lamina and laminate material properties. The polymer matrix is PMT-F7, the material described and tested in the previous section. Testing was carried out on plain weave samples oriented at both ±45 degrees and 0-90 degrees, as well as a laminate with ±45-degree-oriented weaves on the surface and unidirectional axial 0-degree-plies in the middle. The samples were cured in an autoclave at 177 ºC and 97 kPa. After curing, the laminate was sandwiched between G4 fiberglass plates for support and cut into coupons of 5.08 cm in length and 2.54 cm in width using a diamond saw blade. They were painted white with black speckles for DIC strain measurements. The cross section of each sample was micro-graphed to get accurate thickness measurements of the laminates and paint because the paint thickness affected the strain measurements. The bending properties are proportional to the cube of the composite thickness so having an accurate thickness was critical. The test setup and

Table 2. Lamina material properties of the thin-ply composites used in the study.

Material (fiber/resin)	Spread-tow Fabric Form	Width (mm)	FAW (g/m^2)	Ply AW (g/m^2)	FVF (%)	Cured Ply Thickness (µm)	E_1 (GPa)	E_2 (GPa)	ν_{12}	G_{12} (GPa)	Vendor (fiber / resin)
MR60H/ PMT-F7	Unidirectional (UD)	50	38.0	63.4	56	40 ± 3	174.4	8.4	0.259	6.4	Sakai Ovex / Patz M&T
M30S/ PMT-F7	Plain Weave (PW)	1000	61.0	89.7	54	58 ± 3	94.2	94.2	0.026	3.9	Sakai Ovex/ PatzM&T

Table 3. Thin-ply composite laminates labelling, lay-up, average thickness and the number of coupons used in this study

Label	Laminate	# Coupons tested	Avg thickness (µm)
M30S PW_0_x4	$[0\text{-}90PW]_4$	4	228± 4
M30S PW_45_x4	$[\pm45PW]_4$	4	228± 4
LAM1_0_x6	$[\pm45PW_2/0UD_2/\pm45PW_2]$	5	340 ± 15

cycle are shown in Fig 8 (a). To represent loading history conditions similar to the stowage of a boom, the test included four steps. The initial folding step bent the coupon to a set strain/curvature that was representative of the boom during stowage. Once folded, the coupon was maintained at a constant strain while it relaxed for six hours. After relaxation, the coupon was unfolded to a zero-load condition where it was held for the creep recovery step. With 40ºC as the desired stowage temperature, the test was repeated through a series of cycles at higher temperatures. Using the time temperature superposition principle, the 40ºC relaxation response was represented for a desired 2-year time frame with much shorter six-hour relaxation testing times. The bending moment could then be calculated from the measured load and displacement data gathered during the test. Ultimately, the coupon bending stiffness could be calculated with Equation 8. M_{max} is found from Equation 5 and the curvature is the average analytical longitudinal curvature from

Equation 4. This is an effective bending stiffness, D^*_{11} that differs from the true material bending stiffness, D_{11}, because on the CBT test, the boundary conditions applied on the test coupon due to clamping in the fixture offer constrains in additional degrees of freedom, which differs from an the ideal, unconstrained uniaxial bending case. However, D_{11} and D^*_{11} are very similar in most cases

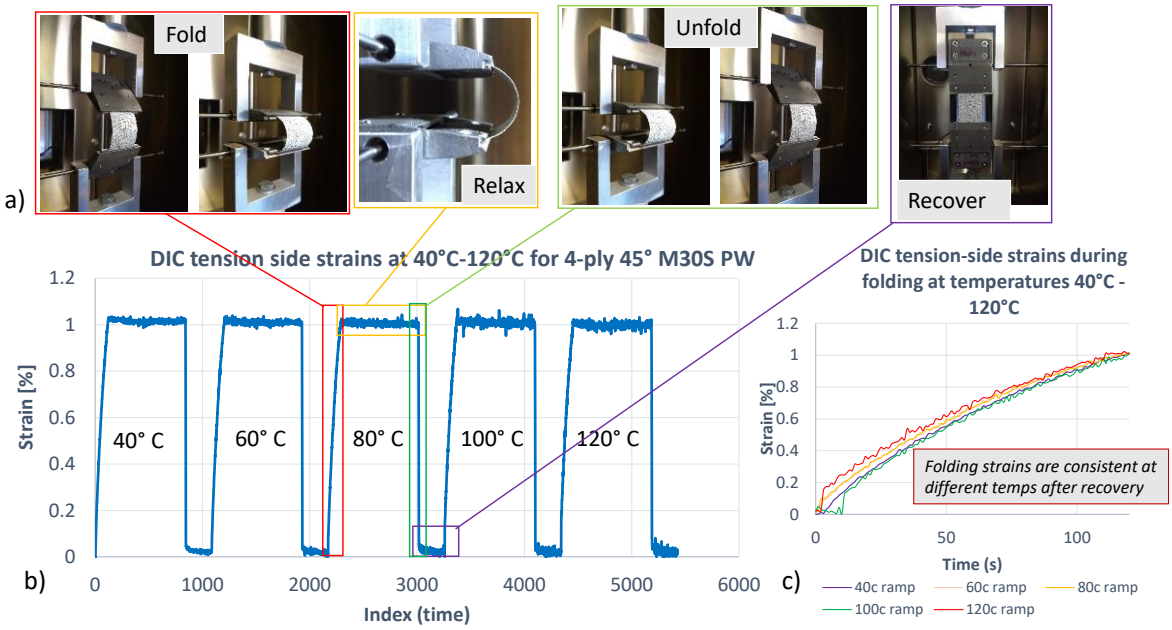

Fig. 8 Thin-ply composite flat coupon bending relaxation test: (a) Fold-relax-unfold-recover cycle applied to the CBT coupon; (b) DIC-measured surface strain cycle at temperatures 40ºC to 120ºC in 20ºC increments; and (c) DIC-measured strains during the folding steps at the different temperatures.

Table 4 Thin-ply Coupon CBT test parameters

Temperature	Thermal steady state time	gage length	expected strain	Fold/unfold time	Relaxation time	Recovery Time	Total test time
40, 60, 80, 100, 120°C	92 min	45pw -27.4 mm 0PW - 34.0 mm Lam1 -35.3 mm	0.9-1%	~2 min	6 h	2 h	48 h

$$D^*_{11} = \frac{M_{max}}{k} \tag{8}$$

The DIC-measured surface strain from a test is shown in Fig. 8 (b). The temperature was increased after each recovery step and held for 92 minutes so the chamber could reach thermal equilibrium. The strain returned to near zero during the 2-hour recovery stage and the coupon was subsequently folded back to the prescribed strain after the temperature was increased and thermal equilibrium was achieved. Figure 8 (c) shows the strains during the folding step for each temperature, indicating that the folding deformation was consistent in this temperature regime, and that negligible permanent deformation was retained in the coupon from the applied cycle. In Fig. 9 the relaxation bending stiffness D^*_{11} for the increasing temperatures is plotted. As expected, the D^*_{11} decreased over time and also decreased as temperature with temperature. Using the TTSP similarly to the polymer tensile relaxation analysis, a master curve can be generated at a relative reference temperature of 40ºC to represent the relaxation bending stiffness D^*_{11} for a longer time at this temperature.

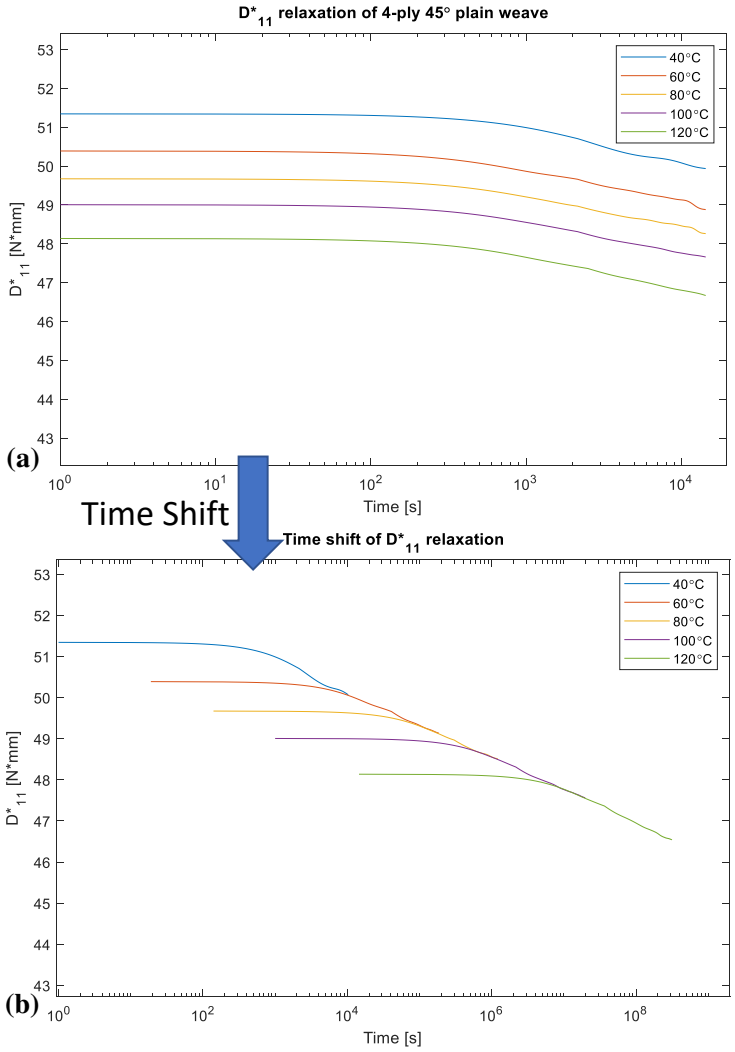

Fig. 9 Effective bending stiffness relaxation, D^*_{11}, at temperatures 40ºC to 120ºC in 20ºC increments for the M30S PW_45_x4 laminate (top) and the master curve at a reference temperature of 40ºC (bottom).

Figure 10 presents all the bending stiffness relaxation master curves at a reference temperature of 40ºC for the three different flat coupon laminates presented in Table 4. There was some variance between samples, most prominently in the LAM1_0_x6 [±45PW_2/0UD_2/±45PW_2] data. The variance was attributed to the spread in coupon thickness, fiber volume fraction and void content. The M30S PW_45_x6 laminates showed the most relaxation followed by the LAM1_0_x6 laminates. During bending, the surface axial strains (around 0.8-1%) were much higher and decreased towards the coupon's neutral axis (0% strain). Therefore, laminates with ±45-degree oriented fibers on the surface experienced a higher relaxation in their bending stiffness since the matrix was highly loaded in shear. The M30S PW_0_x6 laminate had fibers along the bending axis, which lessens relaxation of the polymer matrix as fibers take most of the load, and thus they presented the lowest relaxation. The results from these tests agree with simulations that estimate the fiber volume fraction on the lower end, around 53% [10]. The CBT test, originally designed to study thin-ply composite failure, has been shown to be suitable for testing time dependent properties of thin-ply composites. The CBT fixture was made suitable after iterations on the design to remove non negligible relaxation of the fixture by replacing the polymer clamps with titanium ones via additive manufacturing.

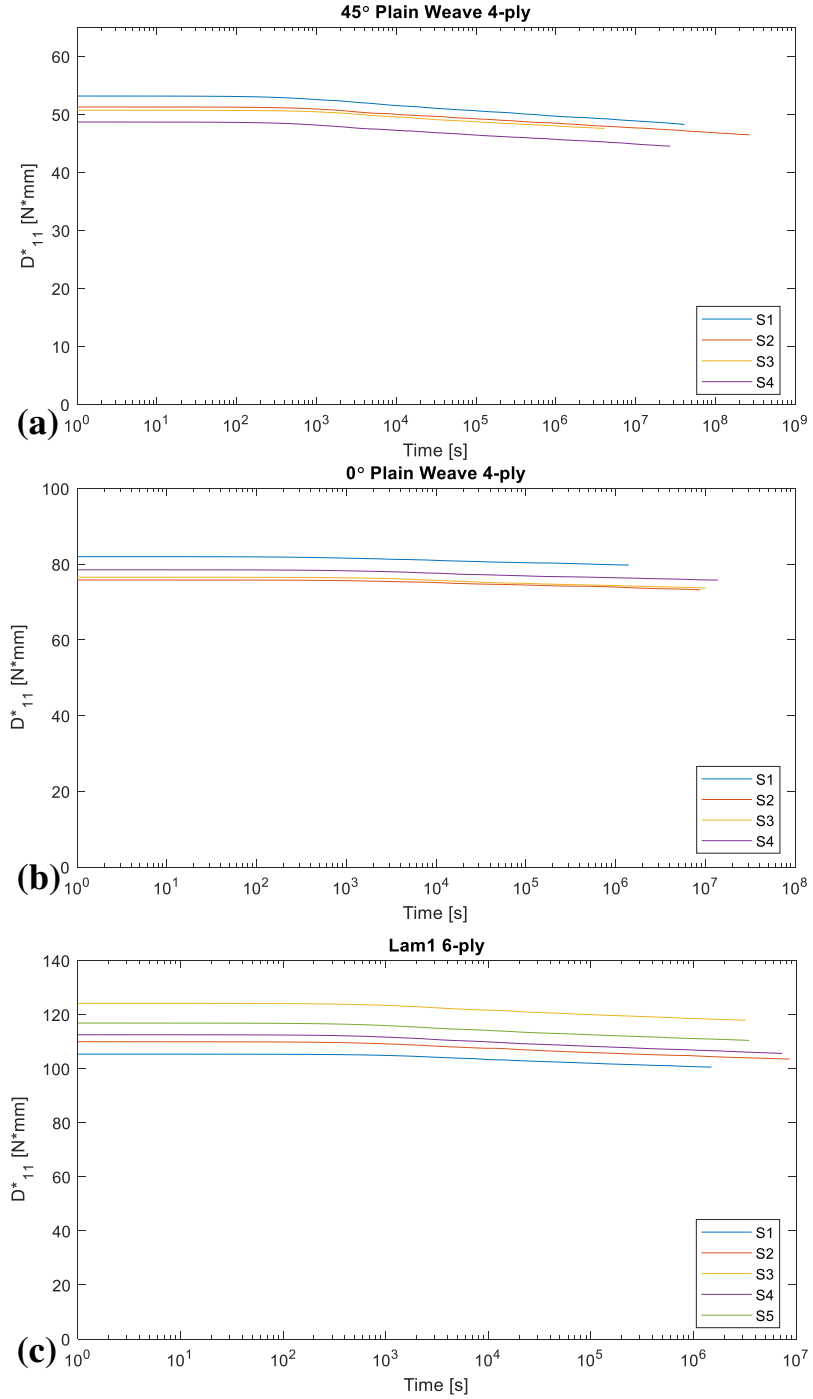

Fig. 10 D^*_{11} Master Curves for the three coupon laminates studied: (a) Four master curves from bending relaxation tests of 4-ply 45⁰ plain weave test coupons (b) Four master curves from bending relaxation tests of 4-ply 0⁰ plain weave test coupons. (c) Five master curves from bending relaxation tests of 6-play Lam1[±45PW$_2$/0UD$_2$/±45PW$_2$] test coupons

IV. Deployable Composite Boom Relaxation Testing

A. Short-Boom Section Column Bending Test

A similar test method to the composite coupon relaxation bending tests was applied to a section of a CTM deployable composite boom. A scaled-up CBT test fixture design was machined from aluminum. This fixture is shown in Fig. 11 (a-b) bending a flattened CTM boom section. The same kinematic relationships (Equations 3-7) apply to this larger fixture. CTM boom sections were cut and painted white with black speckles to capture full-field strain with DIC. The boom sections were flattened and secured on the CBT fixture, and then inserted into a load frame with a thermal chamber to conduct the accelerated bending relaxation test. A similar time and temperature cycle to that of the laminate coupon testing was carried out on the boom sections. A CTM boom was cut into 15.24 cm segments to be placed in the CBT fixture. The test was run at an initial reference temperature of 40 ºC and increased by 5 ºC after 6 hours of relaxation in the folded state and 2 hours of recovery in the unfolded state until 60 ºC. These test parameters are shown in Table 5. The boom was held in the fixture but unloaded for 92 minutes to reach thermal equilibrium. The deformations of the boom section can be split into two separate parts, flattening and bending. Flattening involved bending in the boom hoop/transverse direction and data were not gathered during this instantaneous process. The bending process carried out in the CBT fixture was mainly a uniaxial loading case for the already-flattened two-shelled specimen, where relaxation data was gathered. The strain energy can also be decomposed into these two deformations steps [14]. Figure 11 (c-d) shows there is some cross-sectional flattening deformation after the bending relaxation test. For the CBT test on the CTM section, the calculated bending stiffness did not represent the D_{11} of the associated boom material. Therefore, for these tests it was simply referred to as bending stiffness.

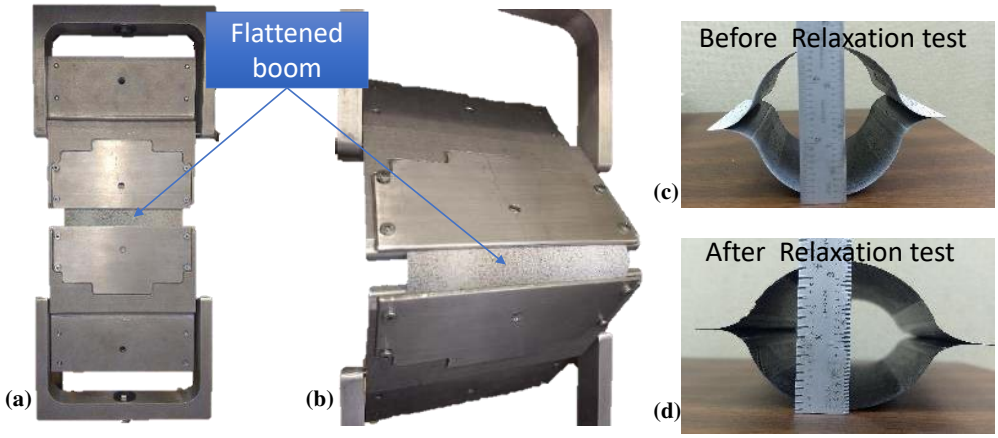

Fig. 11 Relaxation CBT for short-CTM-boom sections: (a) CBT fixture with a flattened 130mm wide CTM boom clamped. (b) CBT fixture bending a CTM boom. (c) CTM boom cross-section before test. (d) Cross-sectional relaxation after the test.

Table 5. Short boom section CBT test parameters

Temperature	Thermal Steady State	gage length	expected strain	Fold/unfold time	Relaxation time	Recovery time	Total test time
40, 45 50, 55, 60	92 min	25.4mm	0.50%	~2 min	6 h	2 h	~48 h

Figure 12 shows the bending stiffness relaxation results from the CBT test of the CTM boom section. The individual relaxation curves at each test temperature are shown in Fig. 12 (a) for boom sample S2 and the time shifted master curve in Fig. 12 (b). The curves were shifted in the time domain to form a master curve at 40 ºC. The bending stiffness master curve of the seven samples are shown in the Fig. 12 (c). There was a 15% variation in the bending stiffness across the seven samples over the relaxation period. The bending stiffness is related to the strain energy stored in the CTM boom section and could be determined and compared to the finite element model-based analysis framework under development that includes the composite material viscoelastic properties [15]. Fig. 12 (d) shows all the TTSP shift factors plotted with their respective tests. The mean shift factors are also shown and were used to calculate equivalent relaxation times at higher selected temperatures for accelerated relaxation test. The shift factors and their corresponding temperatures are shown in Table 6 with the accelerated relaxation times.

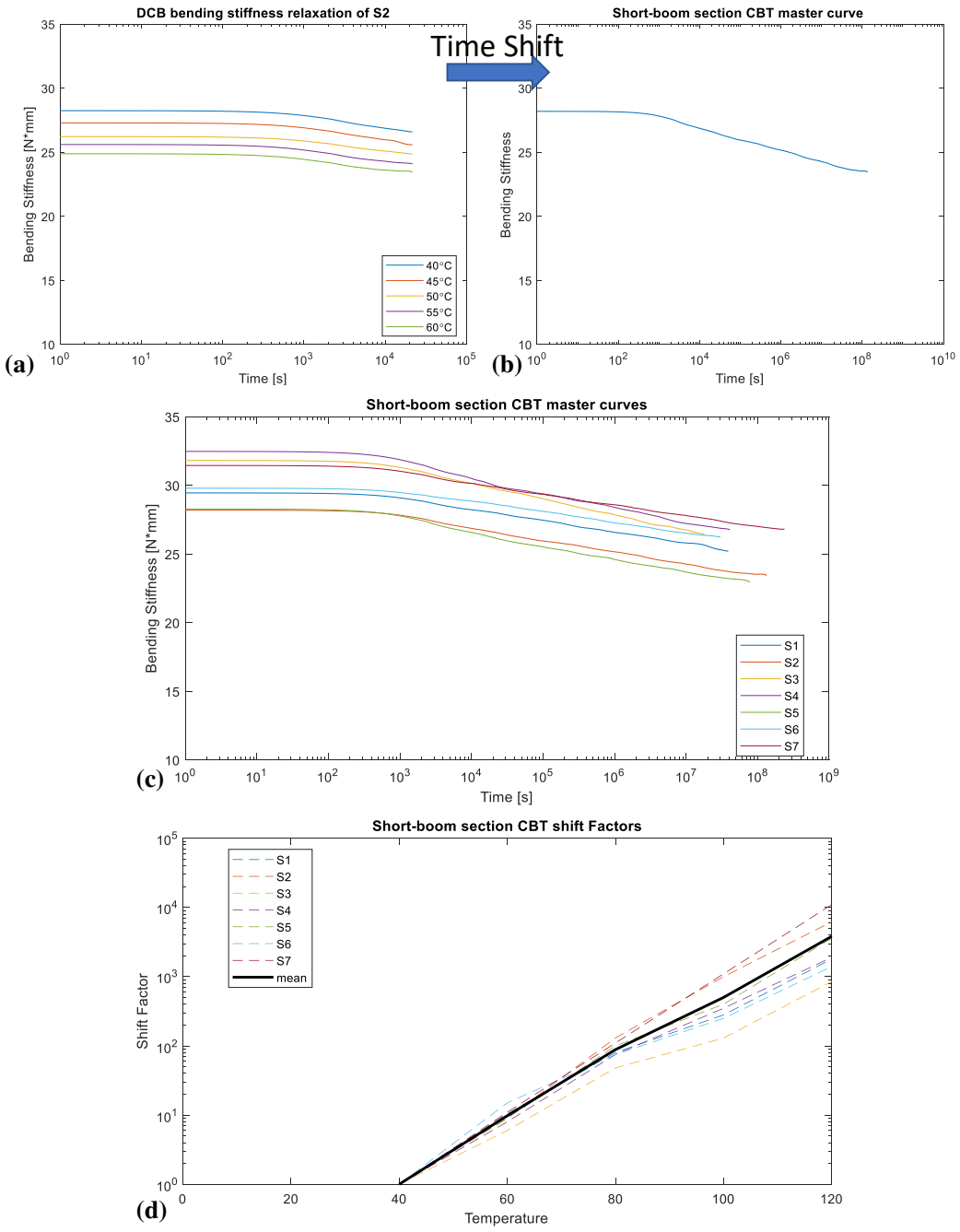

Fig. 12 Relaxation bending stiffness from short-boom section CBT test: (a) Relaxation bending stiffness of sample 2 from 40ºC-60-ºC. (b) Relaxation bending stiffness master curve relative to 40ºC. (c) Master curves of the relaxation bending stiffness for seven short boom sections. (d) Shift factors for the seven bending stiffness relaxation master curves with the mean shift factors.

Table 6. Stowage times based on average shift factors from the short-boom section relaxation CBT

Temperature	Average Shift Factor	1 year in hours	1 year in days	2 years in hours	2 years in days
40	1	8760	365	17520	730
60	9.786	895.182	37.299	1790.365	74.599
80	88.286	99.223	4.134	198.447	8.269
100	501.429	17.470	0.728	34.940	1.456
120	3821.429	2.292	0.096	4.585	0.191

B. Short Boom Section Rolled-up Stowage Test

Short boom segments were tested in the rolled-up stowed operating configuration using the testing fixture shown in Figure 13. As the boom is rolled-up on a spool/hub, the strain energy stored in the boom causes it to self-deploy and/or bloom. The test fixture provided similar boundary conditions to those of commonly used boom deployment mechanisms but was simplified to aid in the analysis of results. This test fixture had seven radial rollers evenly distributed around the boom spool. Each roller was attached to two constant force springs that applied a radial force directed towards the boom spool rotational axis to keep the coiled boom from uncontrollably blooming/blossoming inside the fixture. Three different constant force springs with different forces were used to provide a more uniform force around the packaged boom under gravity since the deployment direction was aligned with the gravity vector. Table 7 shows the resulting force applied to the boom coil at each roller, including the mass of the roller. The diagram on the right of Fig. 13 shows the roller locations and the anti-bloom spring force vectors (in blue) applied to the rollers, as well as the deployment force of the boom that was measured with a load cell attached to the load frame. Two additional static nip rollers also compressed slightly the boom as it exited the test fixture, directing the boom tip to the load cell fitting.

The boom was coiled around a lightweight 180-mm-diameter cylindrical spool. This spool connected to a central shaft that rested on roller bearings to minimize friction. While the boom was stored, the strain energy from the flattened and rolled boom generated a torque on the shaft of the spool. A load cell was attached to the portion of the boom that extended off the spool, measuring the deploying force shown in Fig. 13. As the boom relaxed, the deployment force of the boom decreased in a fashion analogous to the relaxation test carried out on the CBT boom section and flat laminate composite coupons.

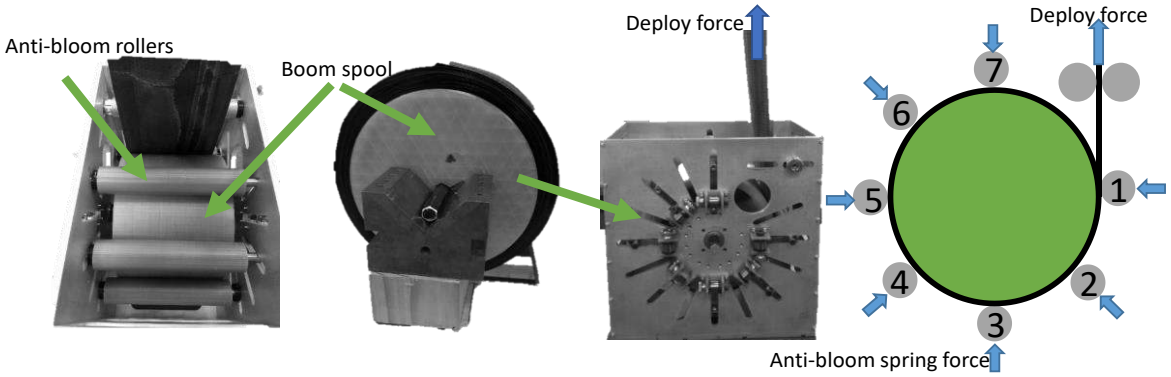

Fig. 13 Full-Scale boom stowage relaxation test fixture showing the anti-bloom rollers and the location of the spool inside the stowage fixture. (right) Diagram showing the spring forces on the anti-bloom rollers and the deploy force of the boom

Table 7. Forces Applied to the radial hub anti-bloom rollers

Roller	1	2	3	4	5	6	7
Force[N]	4.448	3.124438	2.5762	3.124438	2.224	3.547562	3.0283

To accurately determine the deployment force of the boom, the mechanical losses in the test fixture were measured. These losses came from friction and inertia and were determined by testing the fixture with the same dry M30S PW carbon fiber fabric used in the composite boom laminate. The dry fabric material did not store strain energy when coiled on the spool but was expected to have a similar coefficient of friction to the boom samples manufactured. This material was tested with the boom stowage fixture on an MTS electromechanical linear load frame. Figure 14 shows the rolling resistance of the stowage fixture from multiple tests at room temperature, 40 ºC, and 100 ºC. All the test results were consistent. The high temperature of 100 ºC had no noticeable effect on this rolling resistance. Therefore, it was considered that dynamic friction in the fixture was not a critical temperature-dependent parameter, and thus its value could be considered constant in the range of test temperatures. The average resistance of the fixture was 2.39 N. By subtracting the rolling resistance in the test fixture from the load measurement on the load cell that was connected to the spool, the boom deployment force generated from the strain energy of the stowed boom was determined.

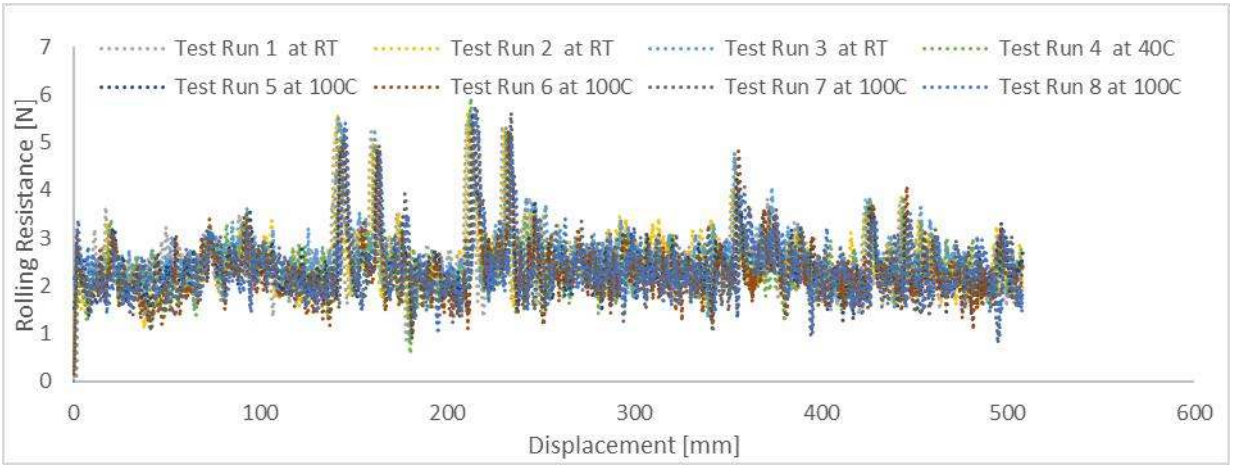

Fig. 14 Rolling resistance of the stowage fixture with dry carbon fiber fabric. 8 tests varying from room temperature to 100ºC all overlapping with similar rolling resistance

After determining the resistance of the stowage fixture, an accelerated stress relaxation of the stowed boom in the fixture was performed. Using the estimated stowage times from the boom CBT relaxation tests shown in Table 6, the stowage temperatures and times were selected for a desired equivalent response for the accelerated relaxation stowage test. Boom sections of about 0.6 m in length were used for initial testing with the stowage fixture. A 0.6-m-long boom allowed for just under one full wrap around the spool. This size was selected for initial testing to avoid additional variance that might have been caused by having boom to boom contact. Tests were performed at 80 ºC and 100 ºC for the time durations shown in Table 6 to represent an equivalent one year of stowage relative to 40 ºC. An additional test was conducted at 100 ºC to represent two years of stowage relative to 40 ºC. The relaxation loads from these preliminary tests are shown in Figure 15.

With the rolling resistance of the stowage fixture accounted for, the initial (zero time) self-deployment force of the boom was between 4.8 N and 6.6 N. The variance in this initial (pre-relaxation) load could be from a combination of variance in the stowage fixture internal forces, the complex self-contact forces of the flattening and rolling of the CTM boom, as well as the surface contact forces of the boom with the spool. These complex interactions caused repeatability concerns in the measurements of both the initial and relaxed boom self-deployment forces. The relaxation of the booms had two higher relaxations for the 100 ºC and 80 ºC 1-year tests, with boom sample S1 tested at 80 ºC relaxing by 13.2% of its initial load and sample S5 tested at 100 ºC relaxing by 14.3%. The 100 ºC 1-year test on boom sample S3 relaxed 5.9% and the 80 ºC 1-year test on boom S2 relaxed 3.9%. These preliminary results have load relaxation spreads close to 10%. The spread is too large to be usable in any boom deployment force analysis. The reasons for the spread in the data could be from complex surface and flattening/rolling interactions between the boom and the spool. There were noticeable dead spots in the booms deployment force where the boom would stop and would be unable to deploy itself. These dead spots could be caused by surfaces and flattening interactions mentioned as well as by bumps at the boom attachment points. Even though the load relaxation data may not be useful the shape recovery post-stowage is still of interest.

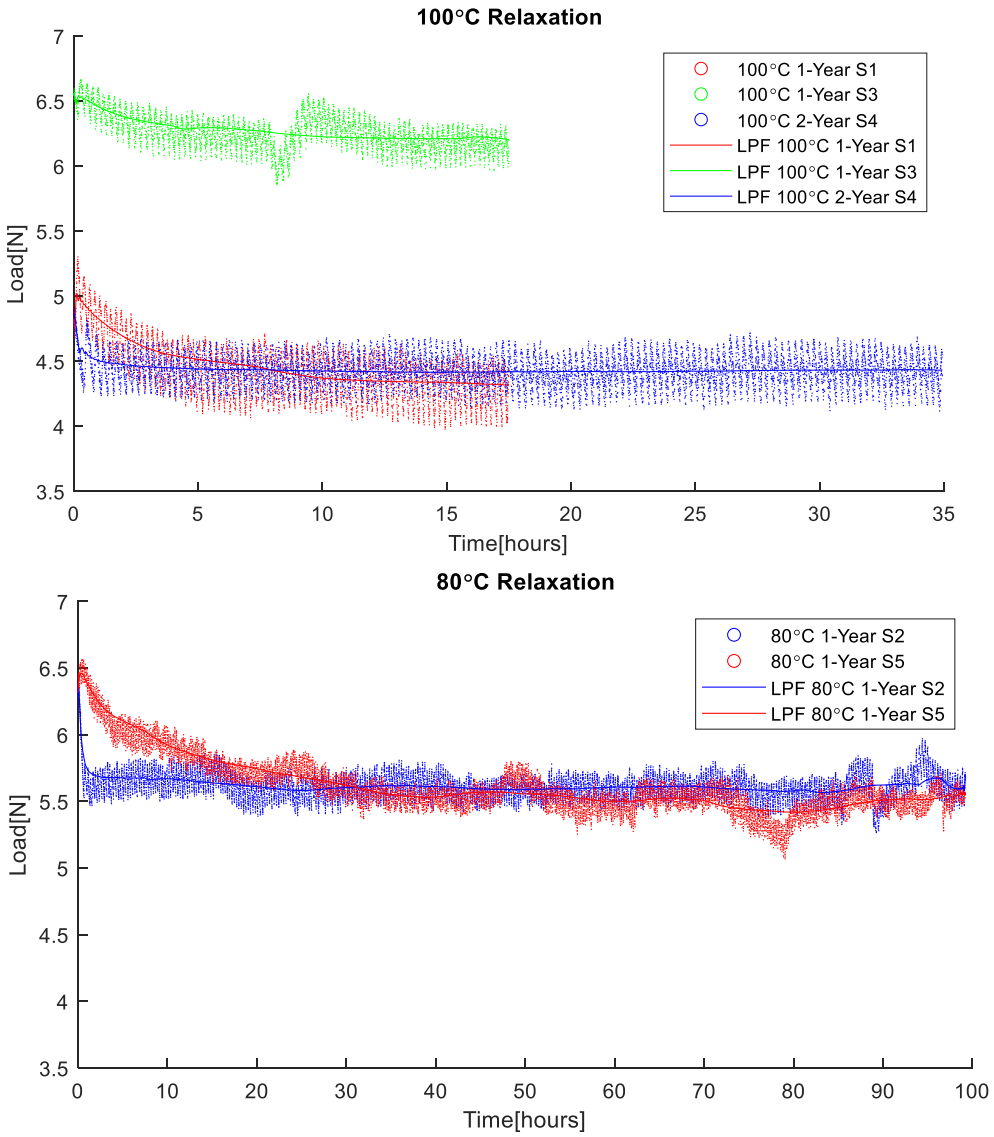

Fig. 15 Deploying force relaxation of the boom during stowage: 100ºC Relaxation (upper plot) with two 1-year accelerated relaxation tests and one 2-year test. Raw data and low pass filtered data shown. 80ºC Relaxation (lower plot) with two 1-year accelerated relaxation tests. Raw data and low pass filtered data shown.

Immediately after the boom stowage test, the boom was placed vertically on a table to minimize gravity effects, and the same quarter shell of the boom was observed for at least 20 hours while its shape partially recovered the pre-stowed geometry. The booms shape recovery was measured with DIC. A quarter of the surface of the booms were initially mapped prior to the relaxation test. The same quarter was imaged during the recovery of the boom. This quarter boom section corresponded to half of the outer shell of the boom (the one that coils on the outside around the spool). The two shell segment radii of the boom section (see Fig. 1 (b)), R1 and R2, were tracked as they recovered over time. The recovery of these two radii, R1 and R2, is shown in Fig. 16. The R1 and R2 values are obtained by taking the average curvature, as measured by DIC, of the shell segment that correspond the locations of the respective radii near the end of the boom that was secured to the hub. The recovery was apparent in both shell segments. In Tables 8 and 9 the boom cross section radii R1 and R2 post-stowage are compared to the pre-stowage dimensions. It is important to note that the nominal values for R1 and R2 are 26.5 mm and 12 mm respectively. The pre-stowed measurements show distortion in these dimensions, most likely from cure induced deformations. Over a 20-hour recovery period most booms recovered close to 50% of their deformation. The single 2-year test conducted at 100 ºC did not have any more significant deformation than the 1-year tests.

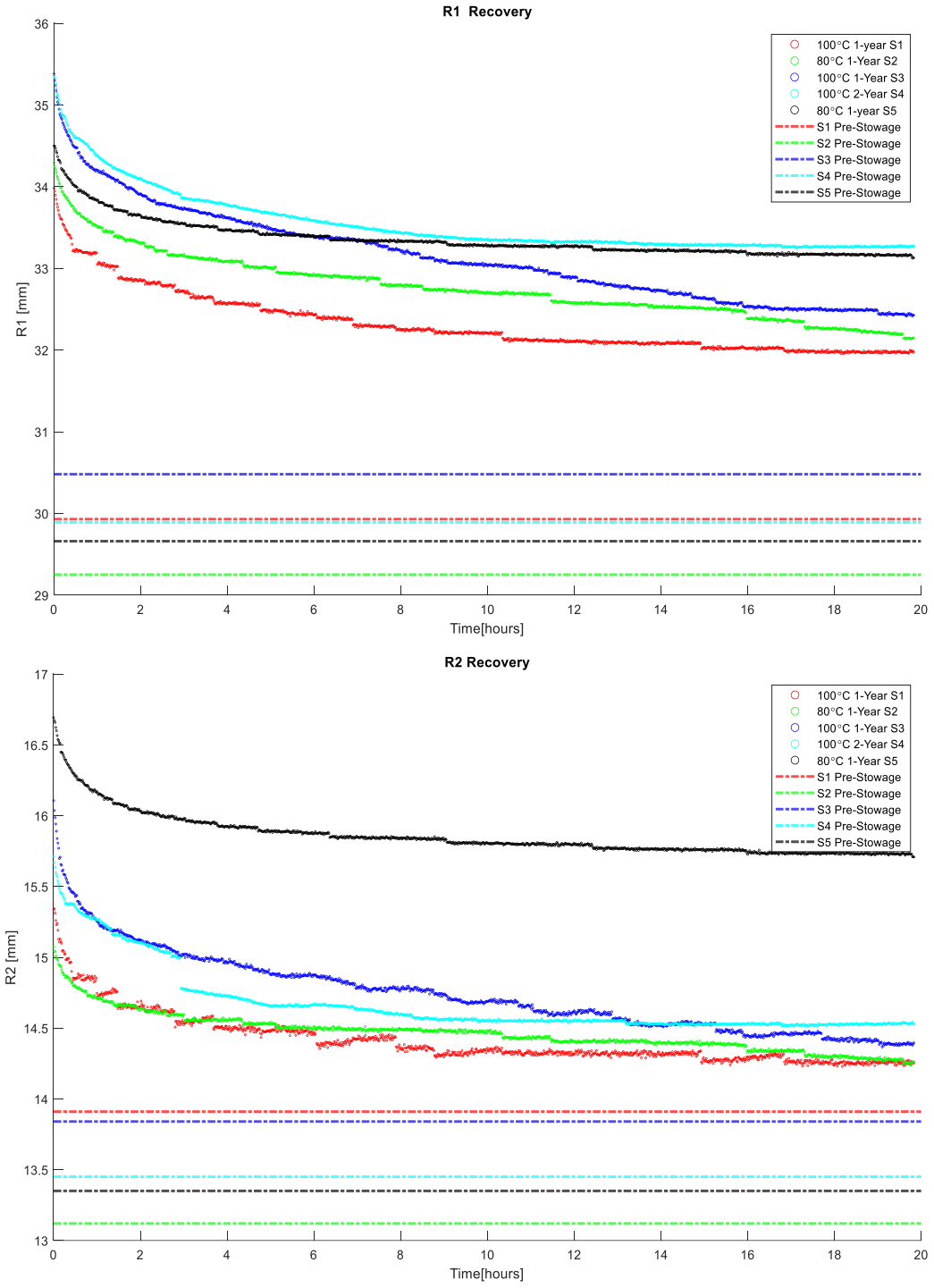

Fig. 16 Radii of the booms pre-stowage and during post-stowage recovery: (Top) R1 and (Bottom) R2 recovery for 20 hours after accelerated relaxation stowage testing and each sample corresponding radius pre-stowage

Table 8. Dimensional recovery of the boom's shell radius R1 compared to pre-stow values

	pre stow [mm]	0hr recovery [mm]	20hr recovery [mm]	% deformed post-stow	% deformed after 20hr recovery
S1	29.93	33.98	31.97	13.52	6.81
S2	29.25	34.29	32.15	17.21	9.90
S3	30.48	35.38	32.43	16.06	6.38
S4	29.89	35.36	33.27	18.31	11.31
S5	29.66	34.5	33.13	16.30	11.68

Table 9. Dimensional recovery of the boom's shell radius R2 compared to pre-stow values

	pre stow [mm]	0hr recovery [mm]	20hr recovery [mm]	% deformed post-stow	% deformed after 20hr recovery
S1	13.91	15.34	14.24	10.26	2.35
S2	13.12	15.07	14.26	14.85	8.67
S3	13.84	16.11	14.4	16.38	4.03
S4	13.45	15.71	14.53	16.81	8.04
S5	13.35	16.69	15.71	25.02	17.68

In Figure 17, surface scan comparisons of the boom segments at different stages in the recovery process are presented. The surfaces are half of the outer boom shell. For each sample, the surface is shown directly after stowage (t=0), and then after 5, 10 and 20-hours of recovery time. The contour surfaces are shown at an isometric viewing angle with the bigger radius R1 above and to the left of R2. The color map on the boom outer shell shows the distance from the mapped pre-stowed shape to the post-stowage shape. The contour scale bar on the left provide the dimensions in millimeters. In the 100 ºC 1-year, S3 boom and the 100 ºC 2-year, S4 boom comparisons, the shells gradually return toward the pre-stowed shape with distance values moving towards zero. The S2 and S5 boom surfaces do not appear to be returning to the original pre-stowed shape. This contradicted their radii recovery measurements shown in Fig. 16. The disagreement here could be from poor global alignment of the pre-stowed and post-stowed booms. The measurements from Fig 16 are locally measured on the boom so they are not affected by global alignments from pre-stowed and post-stowed booms. This information on the recovery of the booms will give insight to their performance after being stowed for long periods of time (1 – 2 years). Furthermore the strain energy from the stowed boom can ultimately be compared to the strain energy of the CBT test carried out on the shorter boom section and to the multi-scale finite element model under development [15] to ensure all forms of testing and analysis agree for predicting the dimensional stability of the boom during a long-term stowage process.

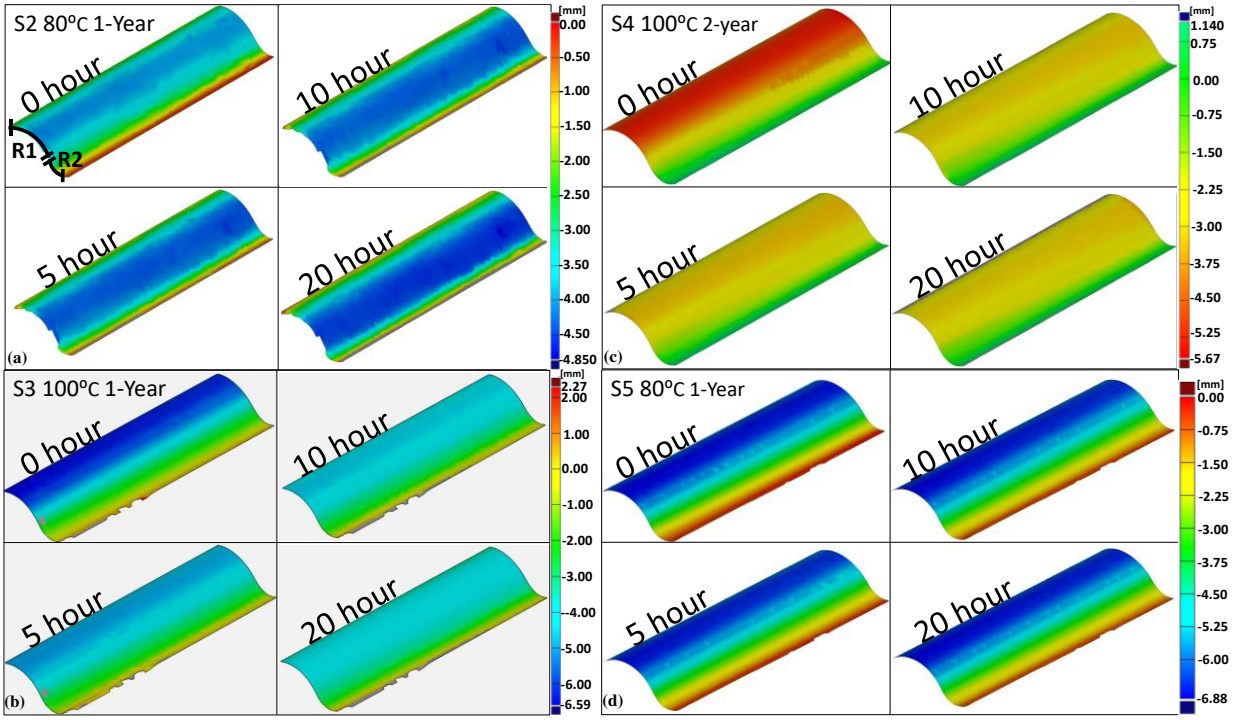

Fig. 17 Surface comparisons of the recovering booms; (a) S2 80ºC 1-year, (b) S3 100ºC 1-year, (c) S4 100ºC 2-year, (d) 80ºC 1-year post-stowage to the booms' pre-stowage surface:

V. Conclusion

Experiments to characterize the dimensional stability of deployable composite booms during stowage have been carried out at a material level, a small-scale structure level and a larger scale structural level. On the material level, time dependent properties of the polymers (PMT-F7 for the resin and EA9696 epoxy for an adhesive) used in deployable composites were tested via tensile relaxation. CBT bending relaxation tests were performed on composite coupons with various thin-ply weaves. Time temperature superposition was used to create master curves of the relaxation of these materials relative to 40 ºC representing relaxation times of up to 2 years. Next small-scale boom structures were tested with a scaled-up CBT. The time dependent relaxation bending stiffness of these structures was characterized with the CBT and used as a baseline for determining the accelerated relaxation testing parameters for full scale boom testing in a custom stowage test fixture. Accelerated relaxation was performed with this stowage test fixture at elevated temperatures to represent 1 and 2 years of stowage at 40ºC.

The rolled-up boom stowage tests were preliminary, and more development and experiments will improve the fidelity of the results. The results from this test do give insight on the deformations that are retained during the stowage of deployable composite booms and how much of that deformation the booms can recover within hours. In future testing, a torque sensor will be used to measure the relaxation of the stowed boom. This will provide a more rigid connection to the stowage test fixture and should give more consistent relaxation data. Even though the rolled-up boom stowage tests results are preliminary the paper has shown a promising multiscale experimental methodology to characterize the dimensional stability of deployable composite booms with direct input to the multiscale analysis framework being developed in parallel [10,11,15]. Future work will compare empirical and computational results for the boom level characterization in order to validate and calibrate numerical models.

Acknowledgments

This research was sponsored by NASA's Space Technology Mission Directorate (STMD) under a Game Changing Development Program (GCDP) project to advance deployable thin-shell composite boom technology [16]. Assistance with boom specimen manufacturing from the Advanced Composites Fabrication Lab technicians at NASA LaRC, Kevin J. Mclain and Mark Griffith, is gratefully acknowledged

References

[1] Fernandez, J. M., Rose, G., Stohlman, O. R., Younger, C. J., Dean, G. D., Warren, J. E., Kang, J. H., Bryant, R. G., and Wilkie, K. W., "An advanced composites-based solar sail system for interplanetary small satellite missions," *2018 AIAA Spacecraft Structures Conference*, 2018, p. 1437.

[2] Stohlman, O. R., Fernandez, J. M., Lappas, V., Hillebrandt, M., Hühne, C., and Straubel, M., "Testing of the Deorbitsail drag sail subsystem," *54th AIAA/ASME/ASCE/AHS/ASC Structures, Structural Dynamics, and Materials Conference*, 2013, p. 1807.

[3] Bosi, F., Schlothauer, A., Leclerc, C., and Pellegrino, S., "Cure-induced deformation of ultra-thin composite laminates," *2018 AIAA/ASCE/AHS/ASC Structures, Structural Dynamics, and Materials Conference*. 2018. p. 2241.

[4] Stohlman, O. R., and Loper, E. R., "Thermal deformation of very slender triangular rollable and collapsible booms," 2016.

[5] Adamcick, B., Firth, J., Pankow, M., Fernandez, J.M., "Impact of Storage Time and Operational Temperature on Deployable Composite Booms", *AIAA Scitech 2020*, Orlando, Florida, January 6-10, 2020.

[6] Fernandez J.M., Krizan S.A., Dyke, E.R. "Thin-Shell Deployable Composite Booms for Solar Sails: Design, Manufacturing, and Qualification", *5th International Symposium on Solar Sailing,* Aachen, Germany, July 31-August 2, 2019.

[7] Kwok, K., and Pellegrino, S., "Folding, stowage, and deployment of viscoelastic tape springs," *AIAA journal*, Vol. 51, No. 8, 2013, pp. 1908–1918.

[8] Kwok, K., and Pellegrino, S., "Micromechanics models for viscoelastic plain-weave composite tape springs," *AIAA Journal*, Vol. 55, No. 1, 2017, pp. 309–321.

[9] Yufei, L., Rique Garaizar, O., Fernandez, J. M., Bergan, A. C., Yu, W., "Multiscale simulation of deployable composite structures", AIAA Scitech 2021 Forum, Nashville, TN, 11-21 January, 2021.

[10] Fernandez, J.M., Salazar, J., Hamillage, M.Y., Gomez-Delrio, Kwok, K., "Large Deformation Bending Relaxation of Thin-Ply Composite Laminates", *22nd International Conference on Composite Materials (ICCM22)*, Melbourne, Australia, August 11-16 2019

[11] Hamillage, Y. P., Kwok, K., Fernandez, J. M., "Micromechanical Modeling of High-Strain Thin-Ply Composites" *AIAA Scitech 2019 Forum*, San Diego, California, January 7-11, 2019.

[12] Fernandez, J. M., and Murphey, T. W., "A simple test method for large deformation bending of thin high strain composite flexures," *2018 AIAA Spacecraft Structures Conference*, 2018, p. 0942.

[13] Sharma, Ajay H., et al. "Analysis of the Column Bending Test for Large Curvature Bending of High Strain Composites." *AIAA Scitech 2019 Forum*, San Diego, California, January 7-11, 2019.

[14] Firth, J. A., and Pankow, M. R., "Minimal Unpowered Strain-Energy Deployment Mechanism for Rollable Spacecraft Booms: Ground Test," *Journal of Spacecraft and Rockets*, 2019, pp. 1–8.

[15] Gomez-Delrio, A. J., Kwok, K., "Stowage and Recovery of Thin-ply Composite Deployable Structures", *AIAA Scitech 2020*, Orlando Florida, 6-10 January, 2020.

[16] NASA Space Technology Mission Directorate, Game Changing Development Program, URL: https://www.nasa.gov/directorates/spacetech/game_changing_development/projects/dcb/